J. Phys. B: At. Mol. Opt. Phys. **32** (1999) 3485–3509. Printed in the UK PII: S0953-4075(99)01104-9

# Elastic scattering and charge transfer in slow collisions: isotopes of H and $H^+$ colliding with isotopes of H and with He

Predrag S Krstić and David R Schultz

Physics Division, Oak Ridge National Laboratory, Oak Ridge, TN 37831-6372, USA

Received 20 January 1999, in final form 10 May 1999

**Abstract.** Differential and integral cross sections are calculated in the centre of mass energy range 0.1–100 eV for elastic scattering of protons ($H^+$, $D^+$, $T^+$) by helium and of symmetric combinations of protons ($H^+$, $D^+$, $T^+$) and hydrogen atoms (H, D, T) by hydrogen atoms (H, D, T). In addition, we derive from the elastic differential cross sections the momentum transfer and viscosity cross sections of use in the study of plasma transport, and compute the charge transfer cross section. Fully quantal and semiclassical approaches are utilized in these calculations, as are very accurate electronic potential energy curves. The results are compared with available data.

## 1. Introduction

Owing to both their fundamental nature and utility for plasma transport studies, we recently reported [1] fully quantal calculations of differential and integral cross sections for elastic scattering and vibrational excitation in low-energy $H^+$, $H + H_2$ collisions. To the same end, we have also presented [2] calculations of the integral elastic cross section and its transport moments (i.e. the momentum transfer and viscosity cross sections) for all isotopic combinations in collisions among hydrogen ions, atoms and molecules, with an emphasis on presenting consistent definitions of the integral cross sections as well as on demonstrating scaling relations among results for these various combinations. As a further aid to plasma modelling, convenient analytical fitting coefficients to describe the differential and integral cross sections were also tabulated [3]. In this work, we present in detail calculations of the differential cross sections for elastic scattering and charge transfer for symmetric isotopic combinations of hydrogen ions ($H^+$, $D^+$, $T^+$) and hydrogen atoms (H, D, T) colliding with hydrogen atoms (H, D, T) and with helium for the range of centre of mass (CM) energies ($E_{CM}$) between 0.1 and 100 eV. The complete database of results covering all of these studies is available through the WWW site of the ORNL Controlled Fusion Atomic Data Center (www-cfadc.phy.ornl.gov).

Here we present (section 2) the formalism appropriate for treating the scattering of quantum mechanically indistinguishable, symmetric nuclei, with particular attention given to the definitions and meaning of the cross sections. We note that considerable confusion in applications of elastic scattering data has arisen due to the difference between the classical and quantum mechanical definitions of elastic scattering and charge transfer for slow collisions involving identical nuclei such as in $H^+ + H$ or $H + H$. The indistinguishability of identical particles results in the inability to distinguish slow protons elastically scattered by H from the recoiling target protons produced by charge transfer, or the slow hydrogen atoms elastically scattered by H from the recoiling H target atoms. This phenomenon is manifested through

0953-4075/99/143485+25$30.00 © 1999 IOP Publishing Ltd 

interference of the wavefunctions for the elastic and charge transfer channels, or for the elastically scattered and recoiled neutral atoms, respectively.

At higher collision energies the overlap of the two channels vanishes, leading to pronounced peaks in the differential cross sections for forward (elastic) and backward (charge transfer or target recoil) scattering. Thus, the elastic cross section defined quantum mechanically tends, at higher collision energies, to the total differential scattering cross section (i.e. the sum of classically distinguishable elastic scattering and charge transfer). At these energies one could calculate or measure the elastic cross section for scattering of the projectile separately from charge transfer or target recoil. Here, we will show that this limit is reached for $E_{CM} > 1$ eV. However, to maintain a quantum mechanically correct definition, consistent with conventions well established in the literature in the energy range considered here, we treat the identical nuclei in ion–atom and atom–atom scattering as indistinguishable, even for $E_{CM} > 1$ eV, when the 'elastic' cross section transitions to the total scattering cross section, containing the non-overlapping sum of direct and recoil channels.

An immediate consequence of this definition is a significantly increased momentum transfer cross section due to its dominant dependence on the magnitude of the differential cross section at large (backward) scattering angles. Therefore, under the assumption of quantum indistinguishability, modelling of particle transport in plasmas should not additionally include momentum transfer through resonant charge transfer, because this is already contained in the total elastic cross section. However, to separate the recoil processes in the integral cross sections for $H^+ + H$, one can subtract the charge transfer cross section from the total elastic cross section, arriving at the elastic cross section in the distinguishable particle sense, which is, of course, well defined only at 'high' energies. Similarly, the elastic differential cross sections may be approximated as the absolute value of the difference of the total and charge transfer differential cross sections. This can then be used to recalculate the integral quantities, such as the momentum transfer and viscosity cross sections, to obtain results that have the right classical limit. We have shown elsewhere [2] that the distinguishability of the particles introduced in such a way does not lead to more than about 10% uncertainty in the integral cross sections for the systems considered here at energies above 0.1 eV.

We also note that the 'spin exchange' cross section defined [4, 5] in the low-energy limit goes smoothly over at high collision energies to the charge transfer cross section defined on the basis of classical distinguishability. In the case of scattering of identical atoms (e.g. H+H), due to the full symmetry of the system, dividing the integral elastic cross section by a factor of two leads to the correct classical limit, but to achieve the same limit in the transport-relevant integral cross sections one needs to separate the forward and backward recoil peaks in the differential cross sections as described above in order to be able to calculate these moments of the elastic cross section.

We present here the results of our calculations based on quantum indistinguishability, assess their accuracy, and compare them with data available in the literature (section 3). In addition to fully quantal results, we have also performed calculations to assess the accuracy of the semiclassical approach in the considered energy range. We have found that no scaling of the differential elastic cross sections for the full range of scattering angles can be discovered in the interval of energies considered relating the different isotopic forms of the constituents of the collision systems. Since all scattering angles contribute in the calculation of the higher moments of the integral elastic cross section a partial or imprecise scaling can significantly deteriorate the accuracy of calculations. Thus isotope-specific calculations for the 15 collision systems ($H^+$+H, $H^+$+D, $H^+$+T, $D^+$+D, $D^+$+T, $T^+$+T, H+H, H+D, H+T, D+D, D+T, T+T, $H^+$ + He, $D^+$ + He, $T^+$ + He) were required. This resulted in the production of more than 900 differential cross sections and 60 integral cross sections (cf [3] and www-cfadc.phy.ornl.gov).

In spite of the high numerical accuracy of the present calculations, the assumption of a weak coupling of the ground gerade ($1s\sigma_g$) and ungerade ($2p\sigma_u$) states with the excited molecular states of $H_2^+$ could result in physical inaccuracies of the differential cross sections for the higher portion of the energy range considered. In particular, it is well known [6, 7] that strong Coriolis (rotational) coupling between the $2p\sigma_u$ and $2p\pi_u$ states at small internuclear distances may influence the cross sections if the product of the collision energy and scattering angle ($E\theta$) is greater than 1 keV degree. We have investigated the influence of this coupling for the ion–atom case, where the consequence of the effect is expected to be more pronounced.

Conclusions regarding the present work are given in section 4. Atomic units are used throughout the text except where explicitly noted.

## 2. Scattering of particles with indistinguishable nuclei

### *2.1. The atom–atom cases: H + H, D + D, and T + T*

In classical mechanics, particles maintain their distinguishability during collisions. This occurs even in such situations as elastic and spin exchange scattering of H(1s) from H(1s) where the particles are identical both before and after the collision, or scattering of $H^+$ from H in which case the incident particles ($H^+$ and H) are identical to either the elastically scattered particles ($H^+$ and H) or those emerging after charge transfer (H and $H^+$). Thus, classically speaking, each of the particles can be labelled and their individual scattering/reaction paths distinguished.

However, in quantum mechanics, identical particles are not always distinguishable and the impact and recoil particle wavefunctions can overlap and thus interfere. If this is the case, the differential cross section will reflect the interference pattern of the two wavefunctions, rather than describe scattering of them separately. At larger collision velocities, as the wavelength of the colliding particles becomes much smaller than the effective interaction region, the particles take on more classical properties. For example, the wavelength of a proton of kinetic energy 1 eV is about 0.1 au. Assuming that the interaction region for scattering from a hydrogen atom in the ground state is about the dimension of the atom ($\sim$1 au), one could reasonably expect the presence of classical distinguishability of elastically scattered particles for this or higher energies. We demonstrate later that this is the case. We also caution that this is not equivalent to saying that classical mechanics may be used to describe elastic collisions at these energies, rather only that classical distinguishability within a quantal scattering treatment is appropriate. As the interference of the two particles diminishes for high collision velocities, the elastic differential cross section in the CM coordinate system shows pronounced forward and backward peaks, characteristic of direct and recoil scattering, respectively, while the interference manifested for intermediate scattering angles vanishes.

To describe such collisions more formally, let us consider the wavefunction of a system of two indistinguishable particles, $\Psi(\vec{R}_1, \vec{R}_2)$. Then the wavefunction obtained from $\Psi$ by interchanging the particles must be physically equivalent to $\Psi$, differing from it by only a phase factor, which yields [8]

$$\Psi(\vec{R}_2, \vec{R}_1) = \pm\Psi(\vec{R}_1, \vec{R}_2). \tag{1}$$

Furthermore, the physical nature of the particles determines whether the system is described by a symmetric or antisymmetric wavefunction. In particular, the total wavefunction of a system of bosons is symmetric, while that for a system of fermions is antisymmetric. The symmetry is defined by the sign of $(-1)^{2\Sigma}$, where $\Sigma$ is the spin of the identical particles. The parity of the total spin of the system, $\mathcal{P} = 2\Sigma, 2\Sigma - 1, \ldots, 1, 0$, defines the symmetry of the spatial wavefunction $\Phi$, i.e. $\Phi(\vec{R}_1, \vec{R}_2) = (-1)^{\mathcal{P}}\Phi(\vec{R}_2, \vec{R}_1)$. Thus, the spatial wavefunction of a

system of two identical particles is symmetric if the total spin is even (singlet, for example), and antisymmetric when the total spin is odd (triplet). Composite particles composed of an even number of fermions (like the deuteron) are bosons while those with an odd number of fermions (the proton and the triton) are fermions with half-integer $\Sigma$. These considerations need to be taken carefully into account in considering low-energy elastic scattering of symmetric systems such as $H^+ + H$ and $H + H$ (and isotopic variants) [8, 9].

Usually, neither the projectile nor target particles are in a definite spin state, the situation being described as scattering of an unpolarized beam of particles of spin $\Sigma$ by an unpolarized gas of target particles. Under these conditions one must average over all possible total spin states, odd and even, assuming that each of the spin combinations has equal probability. Thus, when the total spin is even the cross section is given by [8]

$$\frac{d\sigma_{sym}}{d\Omega} = |f(\theta) + f(\pi - \theta)|^2 \tag{2}$$

and when it is odd, by

$$\frac{d\sigma_{antisym}}{d\Omega} = |f(\theta) - f(\pi - \theta)|^2 \tag{3}$$

where $f(\theta)$ is the elastic scattering amplitude for the CM scattering angle $\theta$ given by

$$f(\theta) = \frac{1}{2ik}\sum_{\ell=0}^{\infty}(2\ell + 1)(\exp(i2\delta_\ell) - 1)P_\ell(\cos\theta), \tag{4}$$

where $k$ is the CM wavenumber, $\ell$ the orbital angular momentum, $\delta_\ell$ the scattering phase shift, and $P_\ell(\cos\theta)$ the Legendre polynomial of order $\ell$.

It follows [9] that the elastic ($el$) cross section for scattering of either of the particles through an angle $\theta$ is, when $\Sigma$ is half-integer

$$\frac{d\sigma_{el}}{d\Omega} = \frac{\Sigma}{2\Sigma + 1}\frac{d\sigma_{sym}}{d\Omega} + \frac{\Sigma + 1}{2\Sigma + 1}\frac{d\sigma_{antisym}}{d\Omega}, \tag{5}$$

and, when $\Sigma$ is integer

$$\frac{d\sigma_{el}}{d\Omega} = \frac{\Sigma + 1}{2\Sigma + 1}\frac{d\sigma_{sym}}{d\Omega} + \frac{\Sigma}{2\Sigma + 1}\frac{d\sigma_{antisym}}{d\Omega}. \tag{6}$$

These formulae are directly applicable to the symmetric scattering of hydrogen atoms (and its isotopes). To begin with, the H(1s) + H(1s) system can evolve both along the $H_2$ ground state singlet gerade $X\,^1\Sigma_g^+$ and triplet ungerade $b\,^3\Sigma_u^+$ molecular states, which are degenerate for $R \to \infty$, where $R$ is the internuclear separation. In particular, two kinds of symmetry are involved in this problem: symmetry with respect to the electronic spins and symmetry with respect to nuclear spins. Thus, the proper symmetrization of the amplitudes with respect to both total electron spin ($\mathcal{P}_e$) and total nuclear spin ($\mathcal{P}_N$) yields scattering amplitudes of the form

$$f(\theta) + (-1)^{\mathcal{P}_N + \mathcal{P}_e} f(\pi - \theta). \tag{7}$$

Since the hydrogen nuclei are fermions of spin $\frac{1}{2}$, we apply equation (5) for both singlet ($\mathcal{P}_e = 0$) and triplet ($\mathcal{P}_e = 1$) states and the subscripts *sym* and *antisym* in the equation are interpreted as the parity of $\mathcal{P}_N$. Thus, we obtain for the electronic singlet case

$$\frac{d\sigma_{el,s}}{d\Omega} = \tfrac{1}{4}|f_s(\theta) + f_s(\pi - \theta)|^2 + \tfrac{3}{4}|f_s(\theta) - f_s(\pi - \theta)|^2 \tag{8}$$

and for the electronic triplet

$$\frac{d\sigma_{el,t}}{d\Omega} = \tfrac{1}{4}|f_t(\theta) - f_t(\pi - \theta)|^2 + \tfrac{3}{4}|f_t(\theta) + f_t(\pi - \theta)|^2, \tag{9}$$

**Table 1.** Parameters for equations (11), (12) defining the elastic differential cross section $d\sigma_{el}/d\Omega$ for neutral-atom–neutral-atom scattering.

| System | $\alpha_s$ | $\alpha_t$ | $\beta_s$ | $\beta_t$ |
|---|---|---|---|---|
| H + H, T + T | $\frac{1}{4}$ | $\frac{9}{4}$ | $\frac{3}{4}$ | $\frac{3}{4}$ |
| D + D | $\frac{2}{3}$ | 1 | $\frac{1}{3}$ | 2 |

where $f_{s,t}$ are given by equation (4) with $\delta_\ell^{s,t}$ the singlet ($s$) or triplet ($t$) phase shifts.

Due to the electron spin statistics, the singlet and triplet contributions to the total elastic cross sections are weighted by factors $\frac{1}{4}$ and $\frac{3}{4}$, respectively, leading to the total differential elastic cross sections for scattering of two H atoms or two T atoms in the form [9]

$$\frac{d\sigma_{el}}{d\Omega} = \frac{1}{4}\frac{d\sigma_{el,s}}{d\Omega} + \frac{3}{4}\frac{d\sigma_{el,t}}{d\Omega} \tag{10}$$

which can be expressed as

$$\frac{d\sigma_{el}}{d\Omega} = \frac{1}{k^2}[\alpha_s\Gamma_s^+ + \alpha_t\Gamma_t^+ + \beta_s\Gamma_s^- + \beta_t\Gamma_t^-] \tag{11}$$

where

$$\Gamma_{s,t}^{\pm} = \left|\sum_{\ell=\pm}(2\ell+1)(\exp(i\delta_\ell^{s,t})\sin\delta_\ell^{s,t}P_\ell(\cos\theta)\right|^2 \tag{12}$$

and + and − mean even values of $\ell$ and odd values of $\ell$ , respectively. For the elastic scattering of deuterium on deuterium, the statistics of the nuclear spins is different, equation (6), since the deuteron, having spin $\Sigma = 1$, is a boson, rather than a fermion. Of course, the statistics of the electron spins is the same as in the H + H and T + T cases. Thus, for D + D we again have equation (10) but with

$$\frac{d\sigma_{el,s}}{d\Omega} = \tfrac{2}{3}|f_s(\theta) + f_s(\pi-\theta)|^2 + \tfrac{1}{3}|f_s(\theta) - f_s(\pi-\theta)|^2 \tag{13}$$

$$\frac{d\sigma_{el,t}}{d\Omega} = \tfrac{2}{3}|f_t(\theta) - f_t(\pi-\theta)|^2 + \tfrac{1}{3}|f_t(\theta) + f_t(\pi-\theta)|^2 \tag{14}$$

which yields the same form as in equation (11). The values of the coefficients $\alpha$ and $\beta$ are shown in table 1 for all of these cases (i.e. for H + H, T + T, and D + D).

Among the most notable work considering elastic scattering in H + H collisions in the literature, Jamieson *et al* [10] introduce an additional factor of $\frac{1}{2}$ in order to adjust the cross section to become identical to that derivable in the high energy, classical limit (Boltzmann statistics). We adopt this convention here as well. Upon integration over the scattering angle, this yields for the total integral elastic cross section [9, 10] for H + H and T + T

$$\sigma_{el} = \frac{2\pi}{k^2}\left[\sum_{\ell=even}(2\ell+1)\left(\tfrac{1}{4}\sin^2\delta_\ell^s + \tfrac{9}{4}\sin^2\delta_\ell^t\right) + \sum_{\ell=odd}(2\ell+1)\left(\tfrac{3}{4}\sin^2\delta_\ell^s + \tfrac{3}{4}\sin^2\delta_\ell^t\right)\right]. \tag{15}$$

The momentum transfer cross section, defined [11] as

$$\sigma_{mt} = \int d\Omega\,\frac{d\sigma_{el}}{d\Omega}(1-\cos\theta) \tag{16}$$

if obtained from equation (10) yields the surprising result that $\sigma_{mt} = \sigma_{el}$. To see this, consider a typical term in the integration in equation (12) which is of the form

$$\int_0^\pi d\theta\ \sin\theta(1-\cos\theta)P_\ell(\cos\theta)P_{\ell'}(\cos\theta) \tag{17}$$

where $\ell$ and $\ell'$ are both either even or odd integers. Using the recurrence relation of Legendre polynomials [12]

$$x P_\ell(x) = \frac{\ell+1}{2\ell+1} P_{\ell+1}(x) + \frac{\ell}{2\ell+1} P_{\ell-1}(x) \tag{18}$$

it follows that

$$\int_0^\pi \mathrm{d}\theta\ \sin\theta\cos\theta P_\ell(\cos\theta) P_{\ell'}(\cos\theta) = \frac{\ell+1}{2\ell+1}\int_{-1}^{1} \mathrm{d}x\ P_{\ell+1}(x) P_{\ell'}(x)$$
$$+\frac{\ell}{2\ell+1}\int_{-1}^{1} \mathrm{d}x\ P_{\ell-1}(x) P_{\ell'}(x) = 0, \tag{19}$$

obtained using the orthogonality of the Legendre polynomials of differing index $\ell$. Since $\ell$ and $\ell'$ are of the same parity, we have $\ell \neq \ell' \pm 1$ always. Thus, since $\mathrm{d}\sigma_{el}/\mathrm{d}\Omega$ contains the symmetry effects, expressed through the separate sums over even and odd partial waves, the part of the integral containing $\cos\theta$ in the integrand of the momentum transfer cross section, equation (14), vanishes, yielding

$$\sigma_{mt} = \sigma_{el}. \tag{20}$$

This differs substantially from the formula

$$\sigma_{mt,Jamieson} = \frac{2\pi}{k^2}\Bigg[\sum_{\ell=even}(\ell+1)\left(\tfrac{1}{4}\sin^2\Delta_\ell^s + \tfrac{9}{4}\sin^2\Delta_\ell^t\right)$$
$$+\sum_{\ell=odd}(2\ell+1)\left(\tfrac{3}{4}\sin^2\Delta_\ell^s + \tfrac{3}{4}\sin^2\Delta_\ell^t\right)\Bigg] \tag{21}$$

with $\Delta_\ell^{s,t} = \delta_{\ell+1}^{s,t} - \delta_\ell^{s,t}$, obtained by Jamieson *et al* [10], starting from the same differential cross section, equation (10), which agrees with the basic definitions of Hirschfelder *et al* [9], for Bose (nuclear) and Fermi (electronic) statistics applied to the scattering of identical particles. Similarly conflicting definitions are applied in obtaining the momentum transfer cross section by Allison *et al* [13].

An alternative definition of the momentum transfer cross section may be considered for H + H scattering at higher energies if one assumes full distinguishability of the projectile and target nuclei (i.e. Boltzmann statistics [9]), and therefore applying only electronic spin statistics. This yields

$$\sigma_{mt,B} = \frac{4\pi}{k^2}\sum_{\ell=0}^{\infty}(\ell+1)(\tfrac{1}{4}\sin^2\Delta_\ell^s + \tfrac{3}{4}\sin^2\Delta_\ell^t). \tag{22}$$

For D + D scattering, assuming distinguishability of nuclei, the Boltzmann-distribution momentum transfer cross section takes on the same form as in the H + H and T + T cases. Moreover, assuming the Boltzmann distribution of nuclei, all differential and integral cross sections take similar forms, irrespective of the type of nuclei.

We note that the viscosity cross section [2] obtained from equation (10) is in full agreement with that obtained by Jamieson *et al* [10] and that we have summarized the formulae for the integral elastic, momentum transfer, and viscosity cross sections elsewhere [2].

### *2.2. The ion–atom cases: $H^+ + H$ and isotopic variants*

The symmetric ion–atom scattering considered here is not scattering of identical particles in the full sense of the phrase since only the nuclei of the colliding partners are identical, and a separate treatment is required. The two possible outcomes of the non-energy changing

**Table 2.** Parameters for equation (30) defining the elastic differential cross section $d\sigma_{el}/d\Omega$ for ion–neutral-atom scattering.

| System | $\alpha_g$ | $\alpha_u$ | $\beta_g$ | $\beta_u$ | $\gamma_{gu}$ | $\gamma_{ug}$ |
|---|---|---|---|---|---|---|
| $H^+ + H$, $T^+ + T$ | $\frac{1}{4}$ | $\frac{3}{4}$ | $\frac{3}{4}$ | $\frac{1}{4}$ | $\frac{1}{4}$ | $\frac{3}{4}$ |
| $D^+ + D$ | $\frac{2}{3}$ | $\frac{1}{3}$ | $\frac{1}{3}$ | $\frac{2}{3}$ | $\frac{2}{3}$ | $\frac{1}{3}$ |

collision are elastic scattering and symmetric charge transfer, in which case the aggregate products of the two processes are indistinguishable. In particular, under the assumption that nuclei are distinguishable, the scattering amplitude representing elastic (direct) scattering in the configuration $A + (B + e^-)$, where A and B are the two protons (or $D^+$ or $T^+$) of the $H^+ + H$ (or, e.g., $D^+ + D$) system is [4]

$$f_d(\theta) = \frac{f_g(\theta) + f_u(\theta)}{2}, \tag{23}$$

where $f_{g,u}(\theta)$ are the scattering amplitudes for the gerade and ungerade ground states, respectively. Similarly, the amplitude for finding the configuration $(A + e^-) + B$ after the collision, i.e. the scattering amplitude for charge transfer (exchange) is

$$f_{ex}(\theta) = \frac{f_g(\theta) - f_u(\theta)}{2}. \tag{24}$$

In the case of identical, indistinguishable nuclei another possible arrangement follows. This situation is obtained if the direction of motion is inverted in the incident wave (e.g., $H + H^+$ substituted for $H^+ + H$). If the direction of the detector is unchanged this also means a change of $\theta$ to $\pi - \theta$ in the amplitudes. In this case, the nuclear singlet and triplet $(s, t)$ components of the differential cross section for the scattering of a proton in the direction $\theta$ are [4, 14]

$$\frac{d\sigma_{el}^{s,t}}{d\Omega} = |f_d(\theta) \pm f_{ex}(\pi - \theta)|^2 \tag{25}$$

where the + sign corresponds to the singlet case and − to the triplet. If we consider the scattering of a beam of unpolarized protons by an unpolarized hydrogen atom target, the elastic differential cross section taking into account the spin statistics of the two identical fermions is [4, 5, 14]

$$\frac{d\sigma_{el}}{d\Omega} = \tfrac{3}{4}|f_d(\theta) - f_{ex}(\pi - \theta)|^2 + \tfrac{1}{4}|f_d(\theta) + f_{ex}(\pi - \theta)|^2. \tag{26}$$

Expanding this definition using the expressions above for the amplitudes we find that the elastic differential cross section can be written in the form

$$\frac{d\sigma_{el}}{d\Omega} = \frac{1}{4k^2}[\alpha_g|\Gamma_g^+|^2 + 3\alpha_u|\Gamma_u^+|^2 + \beta_u|\Gamma_u^-|^2 + 3\beta_g|\Gamma_g^-|^2 + 2\mathrm{Re}\{\gamma_{gu}\Gamma_g^{+*}\Gamma_u^- + 3\gamma_{ug}\Gamma_g^{-*}\Gamma_u^+\}] \tag{27}$$

where $\Gamma_{g,u}^{\pm}$ was defined in equation (12), and the coefficients $\alpha$, $\beta$ and $\gamma$ are given in table 2. Due to the presence of the interference term in this expression, the momentum transfer integral cross section is not equal to the integral elastic cross section [2]. This formula coincides with that reported earlier [2]. As in the case of atom–atom scattering described in the previous section, the formula derived is applicable for both $H^+ + H$ and $T^+ + T$ collisions. The scattering of the deuteron on deuterium must be treated separately since it obeys different spin statistics. Applying a derivation to the scattering of two deuterium atoms we obtain the coefficients given in table 2 for this case.

Similarly, one can define the charge transfer cross section corresponding to the detection of hydrogen atoms in the direction $\theta$ as

$$\frac{\mathrm{d}\sigma_{ct}^{s,t}}{\mathrm{d}\Omega} = |f_{ex}(\theta) \pm f_d(\pi - \theta)|^2. \tag{28}$$

However, if one defined the charge transfer cross section as the flux of hydrogen atoms in the direction $\theta$ for an initially unpolarized incident proton beam, this would contain both recoiled hydrogen atoms and those formed by charge transfer, just as the elastic cross section, equation (26), contains both protons from the projectile beam and from the target. Thus we need somehow to distinguish the hydrogens produced by charge transfer from those elastically scattered. For that purpose we use the nuclear spin for labelling. If the incident flux of protons is polarized (for example of spin $\frac{1}{2}$), and we are able to measure the spin of the protons reaching the detector, the protons of spin $-\frac{1}{2}$ originated in the unpolarized hydrogen target. Thus one defines the cross section for charge transfer involving protons and hydrogen atoms of different nuclear spins, i.e. spin exchange. In this way we are able to distinguish the nuclei of the projectile and of the target by their spin and a result which is the same as in the heteronuclear case (e.g. $H^+ + D$, $T^+ + H$) arises. The spin-exchange cross section is defined by [4, 5, 14]

$$\frac{\mathrm{d}\sigma_{se}}{\mathrm{d}\Omega} = \tfrac{1}{4}|f_g(\pi - \theta) - f_u(\pi - \theta)|^2 = |f_{ex}(\pi - \theta)|^2 \tag{29}$$

where the dependence on $\pi - \theta$ comes from the fact that the detected flux is that of the recoiled target protons. Substituting in the given amplitudes we find

$$\frac{\mathrm{d}\sigma_{se}}{\mathrm{d}\Omega} = \frac{1}{k^2}\left|\sum_{\ell=0}^{\infty}(2\ell+1)\exp(\mathrm{i}(\delta_\ell^g + \delta_\ell^u))\sin(\delta_\ell^g - \delta_\ell^u)P_\ell(\cos\theta)\right|^2. \tag{30}$$

We note that the flux of hydrogen atoms formed from the incident proton beam by charge transfer would be defined as $|f_{ex}(\theta)|^2$ and that the expression one would obtain from a similar analysis for the spin-exchange cross section for symmetric, neutral hydrogen–hydrogen scattering takes exactly the same form [15–18] as equation (28).

It is interesting to consider the behaviour of these cross sections at relatively high collision energies where $f_{g,u}(\theta)$ are sharply peaked in a narrow cone about $\theta = 0$. As a consequence, the overlap of $f_{g,u}(\theta)$ and $f_{g,u}(\pi - \theta)$ is minimal for small $\theta$ and they do not interfere. Then equation (26) can be written in the classical limit as

$$\frac{\mathrm{d}\sigma_{el}}{\mathrm{d}\Omega} \approx |f_d(\theta)|^2 + |f_{ex}(\pi - \theta)|^2 \tag{31}$$

which is the total differential cross section for detecting protons at an angle $\theta$ both by scattering of the beam of protons on the target of H atoms and by capturing electrons from the target atoms, assuming we have a means of distinguishing the scattered and charge transfer fluxes (for example by spin, or by energy). In that case, the charge transfer flux is in a small cone around $\theta = \pi$, while the elastic flux is peaked around $\theta = 0$.

Furthermore, in this classical limit, one can define separately 'pure' elastic ($\propto |f_d(\theta)|^2$) and charge transfer ($\propto |f_{ex}(\theta)|^2$), cross sections. The latter represents the flux of H atoms formed through electron capture to the impacting beam of protons. The corresponding flux of protons $|f_{ex}(\pi - \theta)|^2$, formed by charge transfer in the H target (producing the same integral cross section) would be deflected to angles near $\pi - \theta$. The spin-exchange cross section thus tends to the charge transfer cross section in the classical limit of distinguishability of nuclei, while the elastic cross section in equation (26) leads to the 'total' differential cross section. The energy at which this condition of distinguishability holds is well established (see e.g. [19]) and we find that it occurs for $E_{CM} > \sim 1$ eV. At lower energies the interference between the

elastic and charge transfer channels leads to deviation between the two definitions of the elastic cross section if this separation is performed, the size of which we will discuss in the following section.

For comparison with the symmetric ion–atom and atom–atom collisions that we consider in this work, we have computed as well the elastic cross section for proton ($H^+$, $D^+$, $T^+$)–helium scattering. In this case the particles are completely distinguishable and the differential cross section is calculated simply as potential scattering, i.e.

$$\frac{d\sigma_{el}}{d\Omega} = |f(\theta)|^2 \tag{32}$$

where $f(\theta)$ is defined in equation (4).

## 3. The details of calculation and results

The elastic $S$-matrix element for the $\ell$th partial wave, $S_\ell$, in the absence of inelastic channels, is connected with the relevant phase shift by the relation $S_\ell = \exp i2\delta_\ell$. As discussed above, in all cases considered, the radial functions (from which the asymptotic values of the $S$-matrix are extracted) satisfy uncoupled equations. For example, in the case of H + H scattering the singlet and triplet states are uncoupled, while for $H^+$ + H the gerade and ungerade states are uncoupled. Of course, each of the gerade states may, in fact, be coupled with the excited gerade states, or each triplet may be coupled with excited triplet states. However, these couplings are readily neglected, since at low energies (0.1–100 eV) these are either below the threshold for the reaction or only slightly above, where the transition probability is very small. We have also studied the range of collision energies and scattering angles where these simplifying, though standard, assumptions are justified by considering the rotational coupling of the $2p\sigma_u$ and $2p\pi_u$ states. In the ion–helium case, the dynamics of the elastic collision is determined by a single radial equation of motion on the ground, singlet $H^+$ + He potential curve.

Specifically, the radial equations of motion are

$$\left[\frac{d^2}{dR^2} - \frac{L(L+1)}{R^2} - 2\mu E_a(R) + 2\mu E\right] F_a^{(L)}(R) = 0 \tag{33}$$

where $E_a(R)$ is an adiabatic potential for either the $1s\sigma_g$ or $2p\sigma_u$ state of $H^+ + H$, or either the $X\,^1\Sigma_g^+$ or $b\,^3\Sigma_u^+$ state of H + H. Elastic scattering takes place in each of the uncoupled channels and the total wavefunction has the asymptotic form

$$F_a(\vec{R})|_{R\to\infty} \to \exp(i\vec{k}\cdot\vec{R}) + f_a(\theta)\frac{\exp(ikR)}{R} \tag{34}$$

where $f_a(\theta)$ are the scattering amplitudes for the scattering angle $\theta$. Therefore, we need the adiabatic potential energy curves governing the two colliding particles (found for a series of fixed separations $R$ of the nuclei). This requires the solution of the diatomic eigenvalue problem.

The $1s\sigma_g$, $2p\sigma_u$ and $2p\pi_u$ potential curves can be calculated with arbitrary accuracy owing to the fact that the one-electron–two-centre problem is separable in prolate elliptic coordinates. These curves and their first derivatives were calculated with a step of 0.0002 au for $R \leqslant 1$ and a step of 0.001 for $R \leqslant 50$ to obtain a smooth linear fit used for interpolation in the solution of the radial equations. At larger $R$ (i.e. $R > 50$) an asymptotic expansion up to 11th-order in $1/R$ is used in analytic form [20]. Concerning the H + H system, we have used the best available ground state potentials (both singlet and triplet) provided through private communication by Jamieson [10] based on his extensive compilation and fit of the calculations of Kolos and Wolniewicz [21], slightly modified by us to remove a discontinuity present in

the derivative of the potential. For hydrogen-ion–helium elastic scattering the ground state potential curve was found utilizing a mixed hydrogen–helium Gaussian basis of 34 functions in the Restricted-Hartree–Fock–Full-Configuration-Interaction procedure in GAMESS (General Atomic and Molecular Electronic Structure System) [22], in steps of 0.02 au in $R$ up to 20. For larger values of $R$, the well known polarization potential of He was used.

The introduction of rotational nonadiabatic coupling into the treatment of the ion–atom collisions results in a three-state problem, where only two states ($2p\sigma_u$ and $2p\pi_u$) are simultaneously coupled, by

$$\left[\frac{d^2}{dR^2} - \frac{L(L+1)}{R^2} - 2\mu E_{2p\sigma}(R) + 2\mu E\right] F_b^{(L)}(R) = V_{b-c}^{(L)}(R) F_c^{(L)}(R) \quad (35)$$

where $b$ and $c$ stand for $2p\sigma_u$ and $2p\pi_u$ states and $V_{b-c}^{(L)}(R)$ is the relevant nonadiabatic matrix element.. The independent evolution of the $1s\sigma_g$ state is still described by equation (33). The equations in section 2.2 are still applicable for elastic scattering and resonant charge transfer (spin exchange), while the $2p\pi$ channel carries both additional charge transfer and excitation of the target into the $n = 2$ atomic state. Since this energy-changing channel is distinguishable from the others, the differential cross section for transition into the $2p\pi$ state is given simply by equation (32).

Rotational coupling between the $^3\Sigma_u$ and $^3\Pi_u$ states may also influence the elastic and spin-exchange channels for atom–atom scattering at the high-energy wing of the range considered. Still, this coupling is even weaker than in the ion–atom case due to the smaller 'repulsion' of the relevant molecular terms in the united atom limit of an atom–atom system. Thus, in these cases the deviations found by rotational coupling in the ion–atom systems can serve as a conservative upper bound for the effect of this coupling.

The radial equations for ion–atom and atom–atom systems were solved using the algorithm proposed by Johnson [23] for solution of the stationary Schrödinger equation using the logarithmic derivatives for each partial wave, with $R_{max} = 200$ au in the former and $R_{max} = 30$ au in the latter case, and with $R_{min} = 0.01$ in both cases. The step in $R$ used on the numerical mesh was 0.0001 au. The convergence of the elastic $S$-matrix elements in partial waves was established for each energy by requiring that $\mathrm{Re}\{S_\ell\} \geqslant 0.999\,99$ for at least ten consecutive partial waves. The values of $\ell_{max}$ for a sampling of energies spanning the full range under consideration for some of the ion–atom and atom–atom systems are shown in table 3, including one asymmetric ion–atom and atom–atom case for comparison. We note that a significantly larger number of partial waves is needed for convergence of the ion–atom amplitudes, due to the larger range of the potentials, in comparison with those for the atom–atom amplitudes. The phase shifts for each partial wave were calculated as

$$\delta_\ell = \mathrm{mod}\left(\frac{1}{2}\arctan\left(\frac{\mathrm{Im}\{S_\ell\}}{\mathrm{Re}\{S_\ell\}}\right), 2\pi\right). \quad (36)$$

In order to test its applicability, we also calculated the phase shifts for all 31 collision energies in the range 0.1–100 eV, and for all systems, using the semiclassical expression for the phase shifts

$$\delta_\ell^j = \int_{r_0}^{\infty}\left[k^2 - 2\mu(V_j(R) - \varepsilon_j) - \frac{(\ell+\frac{1}{2})^2}{R^2}\right]^{\frac{1}{2}} dR - \int_{r_0'}^{\infty}\left[k^2 - \frac{(\ell+\frac{1}{2})^2}{R^2}\right]^{\frac{1}{2}} dR \quad (37)$$

where $r_0$ and $r_0'$ are the zeros (turning points) of the first and second integrand, respectively, and $j$ stands for either the gerade or ungerade state in the ion–atom case, and for either the singlet or triplet state in the atom–atom case. The integration was performed for values of $R$ as large as needed to achieve the convergence of $\delta_\ell \leqslant 0.0001$. The convergence in $\ell$ was checked

**Table 3.** Number of partial waves ($\ell_{max}$) needed for convergence of the elastic amplitudes in representative ion– and atom–hydrogen collisions.

| | System | | | | | | | |
|---|---|---|---|---|---|---|---|---|
| $E$ (eV) | $H^+ + H$ | $D^+ + H$ | $D^+ + D$ | $T^+ + T$ | H + H | D + H | D + D | T + T |
| 0.1 | 253 | 306 | 406 | 522 | 57 | 66 | 82 | 102 |
| 1 | 540 | 657 | 863 | 1120 | 130 | 152 | 190 | 241 |
| 5 | 924 | 1121 | 1467 | 1917 | 240 | 283 | 356 | 452 |
| 10 | 1162 | 1409 | 1846 | 2412 | 314 | 371 | 470 | 595 |
| 100 | 2501 | 2920 | 3971 | 5202 | 795 | 938 | 1186 | 1502 |

with a similar accuracy requirement of $\delta_\ell \leqslant 0.0001$. The number of partial waves needed to achieve these convergences is very similar to $\ell_{max}$ in the fully quantal treatment presented in table 3. Furthermore, in the energy range considered, the phase shifts calculated with the fully quantal and semiclassical procedures are almost identical, as are, therefore, the relevant cross sections calculated from them.

The cross sections have been computed for ten points per energy decade at $E_{CM} = 10^{0.1j-1}$ eV, $j = 0, 30$ and the differential cross sections were obtained for 768 values of the CM scattering angle $\theta_m = \frac{\pi}{2}(1+x_m)$ rad, $m = 1, 768$, where $x_m$ is the $m$th zero of the Legendre polynomial $P_{768}(x)$ in the interval $[-1, 1]$. Thus, the $\theta_m$ constitute the set of abscissas for a Gauss–Legendre integration in the interval $[0, \pi]$, used in calculation of the integral cross sections.

A surprisingly small number of elastic cross section data are found in the literature, particularly in the range of energies 0.1–100 eV. As expected, the most detailed work has been done for the $H^+ + H$ system, and we compare here our results for this system with available integral and differential cross sections. We also compare our results with the more sparsely available data for the H + H. Except for $H^+ + D$ collisions [24] we are not aware of any data which are available for comparison with the isotopically modified systems.

Hunter and Kuriyan (HK) made an extensive tabulation of the phase shifts which they obtained from fully quantal calculations of the elastic and charge transfer cross sections [5, 25] for $H^+ + H$. These data are particularly convenient for comparison not only because of their fundamental nature but also because numerical values were tabulated. In table 4 a comparison between the present results and those of HK is given for representative partial waves between 0 and $\ell_{max}$ for 0.1 and 10 eV. For 0.1 eV the lowest values of $\delta_\ell^g$ show better agreement between our quantal and semiclassical data than with the HK results, while all of these results completely agree as $\ell$ increases. For 10 eV, there is good agreement among the three results for all $\delta_\ell^g$; however, for scattering on the ungerade potential, the HK phase shifts occasionally deviate from ours by up to 80%. We attribute this deviation to the lower precision of the potential used by HK, as discussed below.

An examination of the integral cross sections derived from these phase shifts shows generally excellent agreement with HK [24] as well as with the results of calculations by Hodges and Breig [26] (HB). These are shown in figure 1 which includes a comparison of our fully quantal and semiclassical results with the elastic and symmetric charge transfer data of HB and of HK. We also find good agreement with the momentum transfer cross section computed by HB below 10 eV. As would be expected, our semiclassical elastic results differ from the quantal results for energies below 0.1 eV (<6%), but above 0.5 eV they agree to within less than 0.1%. Our quantal results deviate from those of HB by as much as 2% at 0.1 eV but by as little as 0.1% for $E_{CM} > 0.5$ eV. Similar agreement is obtained for the momentum transfer

**Table 4.** Phase shifts from the present fully quantal (QM), present semiclassical (SC) and obtained by quantal calculations of Hunter and Kuriyan [5].

| | QM (present) | | | | SC (present) | | | | HK | | | |
|---|---|---|---|---|---|---|---|---|---|---|---|---|
| | 0.1 eV | | 10 eV | | 0.1 eV | | 10 eV | | 0.1 eV | | 10 eV | |
| $\ell$ | g | u | g | u | g | u | g | u | g | u | g | u |
| 0 | 1.216 44 | 0.026 38 | 3.017 32 | 3.356 21 | 1.216 76 | 0.030 51 | 3.019 43 | 3.354 26 | 1.234 585 | 0.019 202 | 3.023 478 | 4.518 809 |
| 5 | 0.767 34 | 0.626 78 | 3.472 70 | 4.452 44 | 0.767 74 | 0.632 17 | 3.476 01 | 4.450 54 | 0.786 002 | 0.620 891 | 3.479 921 | 4.428 468 |
| 10 | 3.298 28 | 5.900 31 | 2.233 55 | 4.776 20 | 3.298 87 | 5.906 49 | 2.236 18 | 4.774 42 | 3.317 307 | 5.895 139 | 2.239 886 | 4.752 823 |
| 20 | 4.799 54 | 5.474 12 | 2.239 33 | 3.307 03 | 4.803 35 | 5.482 67 | 2.242 24 | 3.305 63 | 4.821 474 | 5.471 833 | 2.245 989 | 3.285 574 |
| 40 | 0.173 59 | 0.165 05 | 0.124 21 | 0.041 72 | 0.173 12 | 0.165 17 | 0.126 10 | 0.041 01 | 0.175 269 | 0.164 588 | 0.131 346 | 0.024 905 |
| 60 | 0.049 90 | 0.049 86 | 5.601 78 | 3.486 76 | 0.049 85 | 0.049 84 | 5.601 96 | 3.486 44 | 0.050 337 | 0.050 155 | 5.608 864 | 3.474 063 |
| 100 | 0.010 82 | 0.010 81 | 0.236 42 | 0.857 10 | 0.010 81 | 0.010 81 | 0.234 19 | 0.857 10 | 0.010 871 | | 0.241 409 | 0.850 499 |
| 200 | | | 0.502 62 | 6.080 38 | | | 0.501 92 | 6.080 41 | | | 0.502 988 | 6.080 018 |
| 300 | | | 0.055 12 | 0.028 35 | | | 0.055 05 | 0.028 35 | | | 0.064 165 | 0.037 268 |

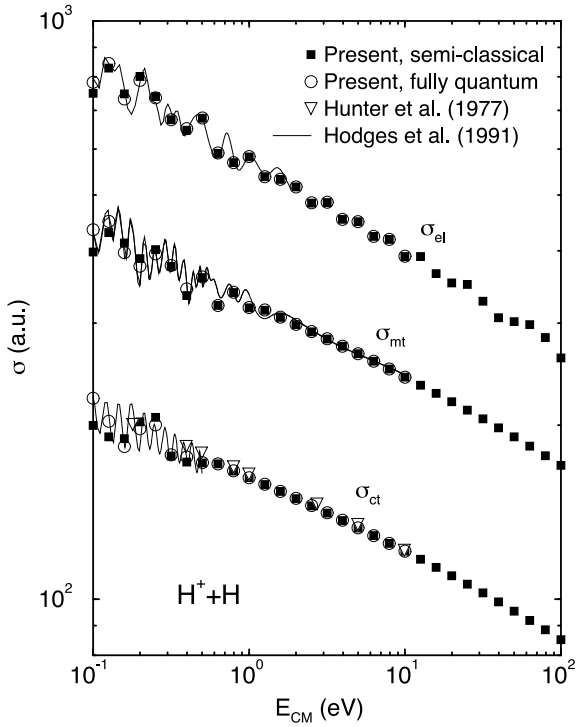


**Figure 1.** Integral elastic ($\sigma_{el}$), momentum transfer ($\sigma_{mt}$), and charge transfer ($\sigma_{ct}$) cross sections in collisions of proton and atomic hydrogen.

cross section, i.e. our quantal data agree with HB to within 0.1% at 0.1 eV, but the difference varies irregularly toward higher energies. We attribute the disagreement to the imprecision of our digitizing procedure used to obtain the data from the published diagrams of HB which may be expected to introduce on the order of 2–3% uncertainty into the comparison.

The dispersion of the symmetric charge transfer data shown by the four sets of integral cross sections is larger than that for the elastic channel at the lowest energies. Specifically, our semiclassical data deviate by about 10% from the fully quantal calculations at 0.1 eV. This difference drops to below 0.05% at 0.5 eV. The HB charge transfer cross section differs by about 6% from our quantal calculation, and this difference drops with energy (<3% at 0.5 eV, and <1.5% for 1 eV). Similarly, the HK data differ from ours by 4% at 0.1 eV, which drops to less than 1.2% at 0.5 eV. The HK data apparently differ even more from the HB results since their deviations are in opposite directions from our data. Still, we stress that in this case both sets of referenced data were obtained by digitizing the published data, which can introduce an error of a few per cent. We also note that there are no published quantal viscosity cross section data for this system.

HK [5] also provided a comprehensive set of differential cross section data for the low-energy range. The deviation of their elastic differential cross section from our fully quantal results at 0.1 eV is within the errors of digitization, as can be seen in figure 2. The deviation of our semiclassical data from the quantal results is larger than the deviation from HK's results, especially at large angles, as expected. However, for $E_{CM} = 0.1$ eV, the semiclassical data reflect in full the correct structure of the differential data (positions of the peaks), underestimating the peak values by only a few per cent. Moreover, at a collision

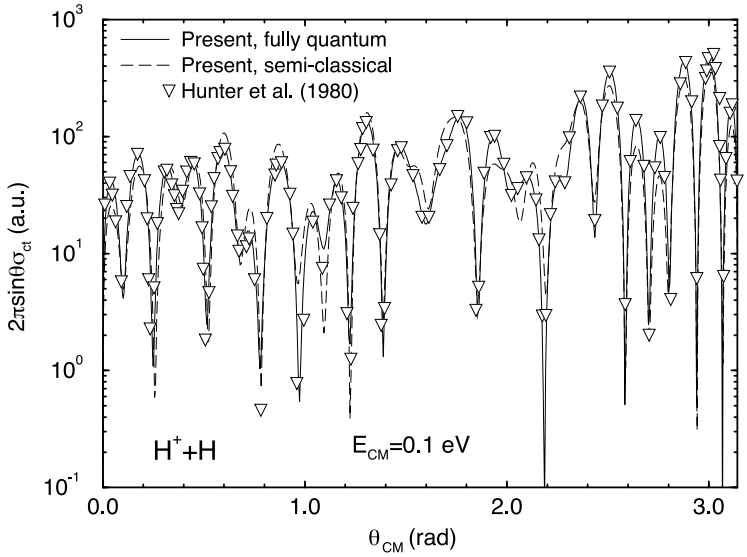


**Figure 2.** The elastic differential cross section at $E_{CM} = 0.1$ eV for proton–hydrogen scattering.

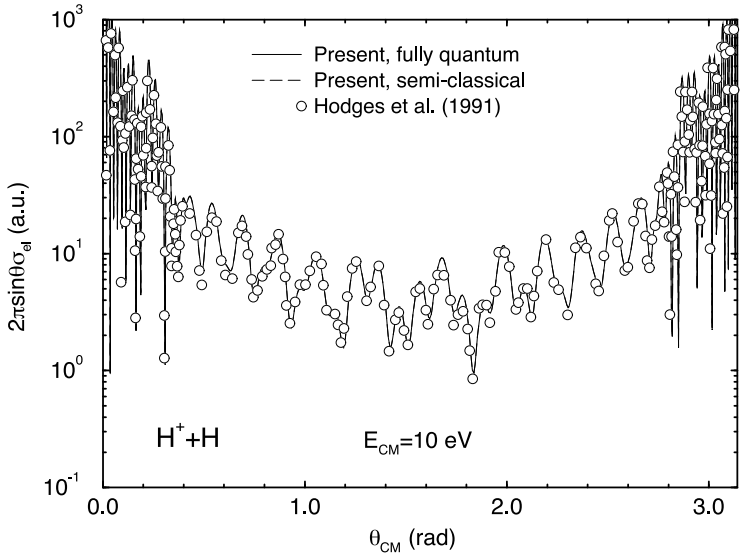


**Figure 3.** The elastic differential cross section at $E_{CM} = 10$ eV for proton–hydrogen scattering.

energy of 1 eV, there is no discernible deviation between our quantal and semiclassical elastic differential cross sections, while any significant difference between them and the data of HK (not shown) can be attributed to the digitization errors. This is also shown in figure 3, which compares the present results with those of HB for 10 eV.

An assessment of the accuracy of the present results compared with those of HK and HB can be made by considering the details of each calculation. In particular, the calculation of HB essentially repeats the calculation of HK [25] with only slight modifications, using the HK tabulated adiabatic potentials (67 values in the interval of $R$ between $\frac{1}{64}$ and 50 au), and uses

the same procedure for integration of the radial Schrödinger equation (Numerov method). The values of the potentials needed were then found by cubic spline interpolation. For $R$ greater than 50 au, a polarization potential ($\propto 1/R^4$) was used to find the values for both gerade and ungerade potentials. At large $R$, HK used an analytic approximation to the solution of the radial equation, while HB solved it numerically. Extensive checks of the convergence were performed by HB, leading to somewhat different values of $\ell_{max}$, as well as a slight disagreement of the two sets (HK and HB) of the elastic and charge transfer cross sections.

In the present work, we calculated the gerade and ungerade potentials with eight-digit accuracy at $10^5$ points from $R = 0.0002$ to 50 au, thus reducing the error in interpolating the potentials at the points required by the numerical solver. For larger distances, we used the asymptotic expansion for the adiabatic potentials up to 11th order, rather than only up to 4th order. Our numerical procedure was based on Johnson's algorithm with logarithmic derivatives, which achieves a better accuracy and a better numerical stability than the Numerov method. Finally, our convergence criteria were more stringent than those in the other works. Specifically in our calculation we required a 2–3 times greater number of partial waves. For example, at 0.1 eV we used 253 partial waves, while HB used 120 and HK used 147. At 5 eV we used 924, while HB used 340 and HK 300 partial waves. For 10 eV HB used only 420 partial waves while our convergence criteria required 1162. These increased numbers of partial waves and more accurate long-range potentials resulted in an increased accuracy in the differential cross sections especially for small scattering angles. An estimate of the maximum relative error of our quantal results for the differential cross sections for elastic scattering and charge transfer in $H^+ + H$ collisions yields a value of $10^{-7}$. Nevertheless, this is not necessarily a physical result accurate to seven digits since neglect of the nonresonant, inelastic channels may significantly reduce this accuracy, especially at higher energies, where these channels open.

In figures 4 and 5 we compare our fully quantal and semiclassical results for the integral elastic, momentum transfer, and viscosity cross sections for $H^+ + He$ and $H^+ + H$ with the classical results of Bachmann and Reiter [27]. Two factors may significantly influence the reliability of the elastic cross sections obtained by classical calculations. First, classically, the colliding particles are distinguishable, even if they are identical. This is not correct for $H^+ + H$ at low collision energies and can only be resolved by an adequate quantum mechanical treatment. Second, the elastic cross section cannot be properly defined within classical mechanics, unless the interaction potential is of finite range. That is not the case here, and thus the classical integral elastic cross section is infinite. In order to render a finite result one must introduce a cutoff in the classical deflection function. A high degree of arbitrariness in the choice of cutoff may introduce significant errors in the results. Unlike the elastic cross section, both momentum transfer and viscosity cross sections are finite even classically, if the interaction potential decreases at large distances faster than the Coulomb one. This is the case for the present systems, and one can expect reasonable results even classically.

For $H^+ + He$, the classical momentum transfer and viscosity cross sections, consequently, agree reasonably well with the quantal values, while the elastic results deviate by a larger amount. The present results for the $H^+ + H$ case include identity of the nuclei and thus indistinguishability of the protons coming from the elastic scattering and from charge transfer. As a consequence, the quantum mechanical momentum transfer cross section is significantly larger than the classical one, as shown in figure 5. The momentum transfer cross section is mostly influenced by elastic scattering in the backward direction. This scattering is significantly smaller in the case of distinguishable particles, since backward scattering is mixed with the charge transferred protons. This explains why our result has such a significantly different momentum transfer cross section from the classical one. The viscosity cross section, being

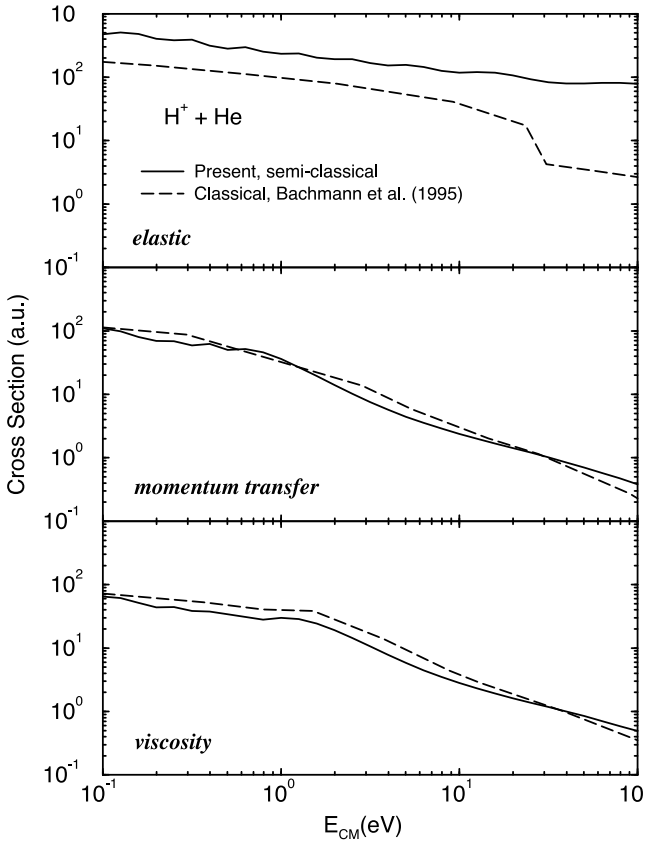


**Figure 4.** Comparison of the present calculated results for the integral elastic, momentum transfer, and viscosity cross sections describing proton–helium collisions with the classical results of Bachmann and Reiter [27].

dependent on angles around $\frac{\pi}{2}$ rad, is in reasonable agreement with the classical calculation. We also show in figure 5 the analytical result of the semiclassical Massey–Mohr approximation (see e.g. [28]) with distinguishable particles.

Little attention has so far been given to the study of elastic collisions between neutral hydrogen atoms in the presently considered energy range. For example, the range of energies between 0.1 and 100 eV is somewhat above that of interest for many astrophysical applications and below the range of energies where inelastic processes compete with the elastic ones. In addition, experiments seeking to observe the scattering of neutral hydrogen atoms are very difficult, and thus the data available are sparse even at higher or lower energies. As a consequence, we can compare our data with only few calculations, and these are mostly oriented to the astrophysically interesting spin-exchange process. Figure 6 shows our elastic data compared with one point of Koyama and Baird [15]. Since this point is at low energy (1000 K), far from our energy range, we use the previous semiclassical calculation of Schultz *et al* [28] to extend our curve toward lower energies. At keV energies we display the results obtained by Flannery *et al* [29], indicating that at higher energies, where inelastic processes start to play a significant role, the elastic cross section might experience a significant drop. Concerning the spin-exchange cross section, our results are in reasonable agreement with those of Dalgarno [16] and of Hayden *et al* [30], as well as in excellent agreement with the previous

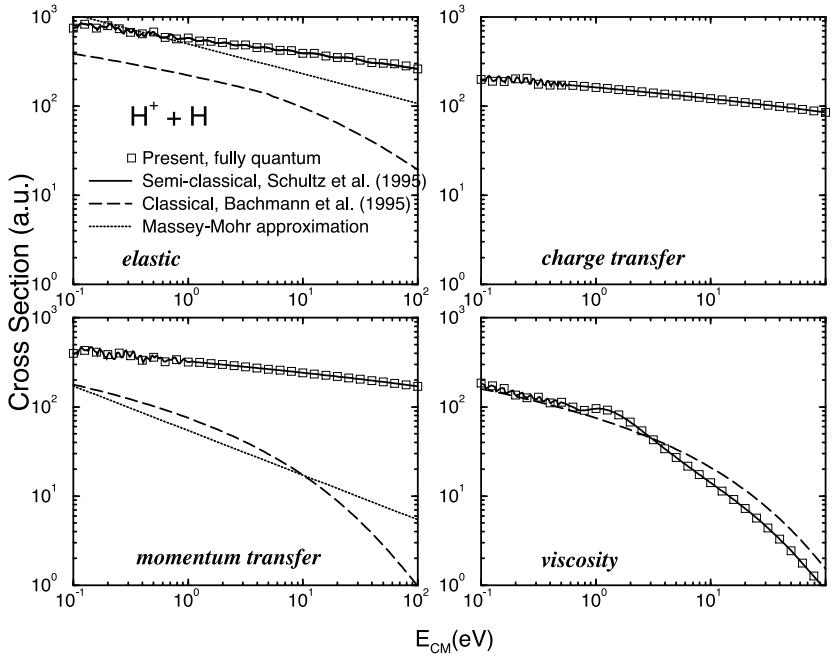


**Figure 5.** Comparison of the present calculated results for the integral elastic, momentum transfer, charge transfer, and viscosity cross sections for proton–hydrogen collisions with the classical results of Bachmann and Reiter [27].

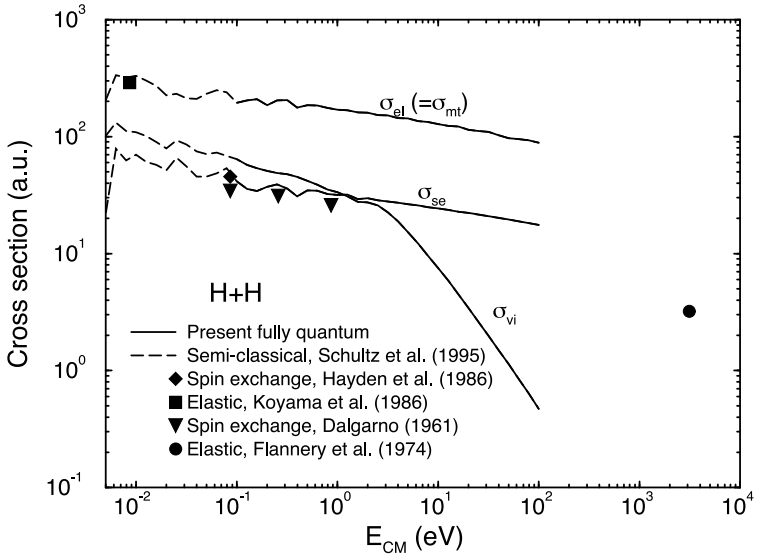


**Figure 6.** Comparison of the present results for the integral elastic, momentum transfer, viscosity, and spin-exchange ($\sigma_{se}$) cross sections in collisions between hydrogen atoms.

semiclassical calculations of Schultz *et al* [28], all also shown in figure 6.

Details of the atom–atom (H + H, D + D, and T + T) and ion–atom ($H^+$ + H, $D^+$ + D,

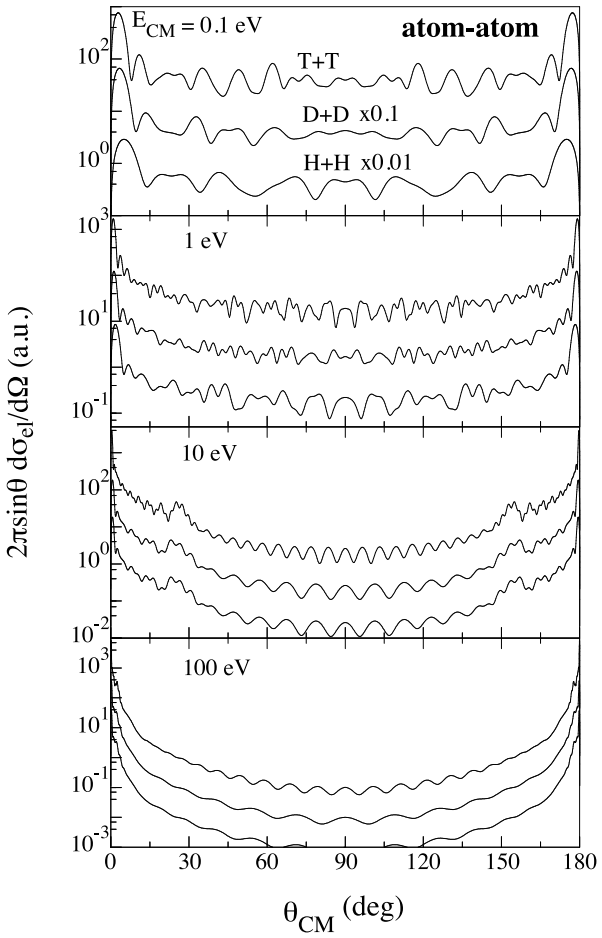


**Figure 7.** The differential elastic cross section for various isotopic combinations of H + H, at representative CM collision energies.

and $T^+ + T$) elastic differential cross sections for representative collision energies are shown in figures 7 and 8, respectively. The complete symmetry around the scattering angle of 90° for the neutral–neutral systems, is only an approximate symmetry for ion–atom systems. We have shown elsewhere [2] that charge transfer (recoil peak) contributes about 40% of the cross section. For H + H, the recoil peak contribution is exactly 50%. A much larger number of partial waves takes part in the ion–atom case due to the long range of the polarization potential, which causes a larger number of oscillations in the differential cross section as well as a larger value of the forward peak than for the atom–atom case. The forward peak in the $H^+ + H$ case is about two orders of magnitude above the cross sections for the intermediate angles for lower energies, while this is only an order of magnitude for the H + H case. This is mainly due to an order of magnitude smaller forward peak value of the neutral–neutral in comparison to the ion–neutral system, while the region of the intermediate angles is mainly independent of the projectile charge and mass or target mass, except for the oscillation details. As a consequence, mixing of the direct and recoil peaks and thus quantum effects for the neutral–neutral systems are more pronounced at lower energies than in the ion–atom cases.

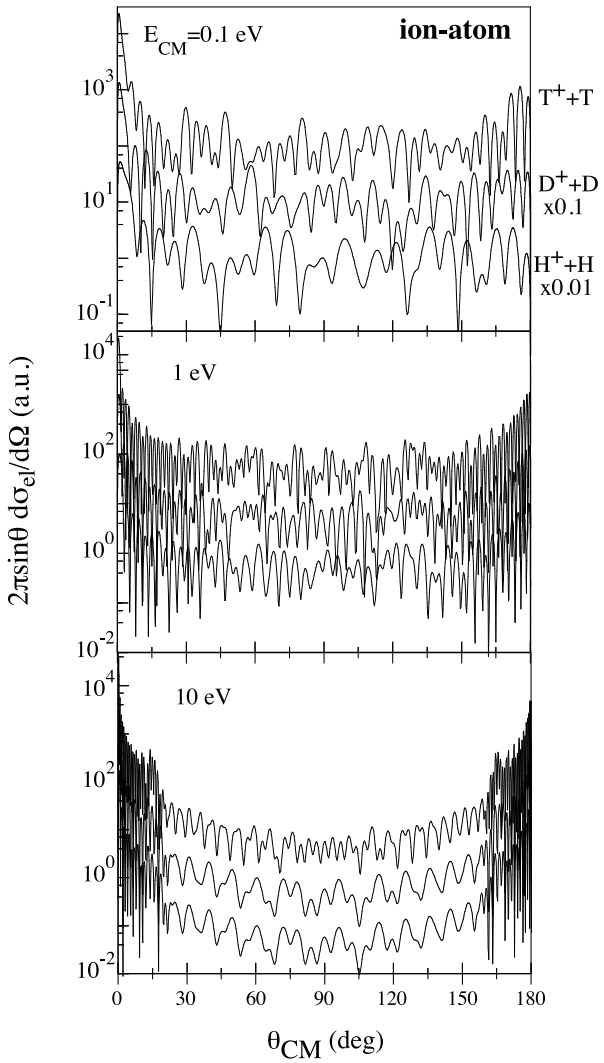


**Figure 8.** The differential elastic cross section for various isotopic combinations of $H^+$ + H, at representative CM collision energies.

As discussed above, for sufficiently high collision energies the $2p\sigma$–$2p\pi$ coupling, active for small internuclar distances, may have a sizable effect on the elastic differential cross section. As seen in figure 9 for $H^+$+H, the influence of this transition is small for energies $E_{CM} \leqslant 50$ eV. Increasing with the energy and simultaneously decreasing with the reduced mass of the system, the deviation of the two curves at $E_{CM} = 100$ eV is present for intermediate scattering angles, where the cross section is small. As a consequence, the integral elastic cross section is only weakly influenced by inclusion of the rotational coupling. The largest deviation is present for the viscosity cross section, which is dominantly built up by the differential cross section at intermediate scattering angles. This is confirmed in figure 10, where the relative deviation for various integral cross sections is shown as a function of energy. The deviation for the elastic cross section is slightly larger than 1% at 100 eV, while for the viscosity cross section it

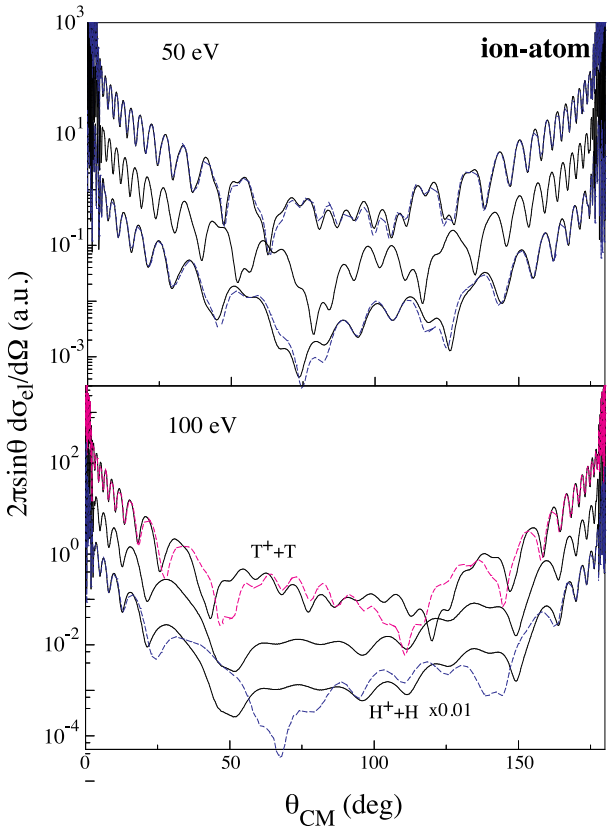


**Figure 9.** The differential elastic cross sections for various isotopic combinations of $H^+ + H$ in the absence (solid) and in the presence of the $2p\sigma_u$–$2p\pi_u$ rotational coupling (dashed curves).

reaches more than 3%. The momentum transfer cross section for this indistinguishable-nuclei collision is almost entirely due to the 'charge transfer' contribution in the elastic cross section and thus, the correction to the momentum transfer and charger transfer cross sections caused by rotational coupling almost overlap, not exceeding 2.5% at $E_{CM} = 100$ eV (figure 10).

Another interesting comparison is shown in figure 11, illustrating the relative behaviours of the spin-exchange and charge transfer differential cross sections for neutral–neutral (D + D) and ion–neutral ($D^+$ + D) cases. This figure shows the significant large-angle scattering in these collisions and the expected greater magnitude of the ion–atom charge transfer cross section. The influence of the rotational coupling on the charge transfer cross section is shown in figure 12 for $E_{CM} = 100$ eV, where the differential cross sections for charge transfer via the $2p\sigma$ state (into the ground state of H) and the charge transfer + excitation cross section via the $2p\pi$ state are shown. The influence of the $2p\sigma$–$2p\pi$ coupling is noticable only for intermediate angles, where the charge transfer cross section is small.

As shown in figure 13, in ion–helium ($H^+$, $D^+$, $T^+$ + He) collisions, the backward peak observed for ion–hydrogen scattering in figure 8 is absent. This occurs because the projectile and the target are completely distinguishable and consequently the direct elastic scattering is a well defined quantity at all energies. While the peak value of the cross section is almost independent of energy, the scattering angle corresponding to the peak moves toward lower angles with increasing energy, thus decreasing the peak width and the effective area (integral

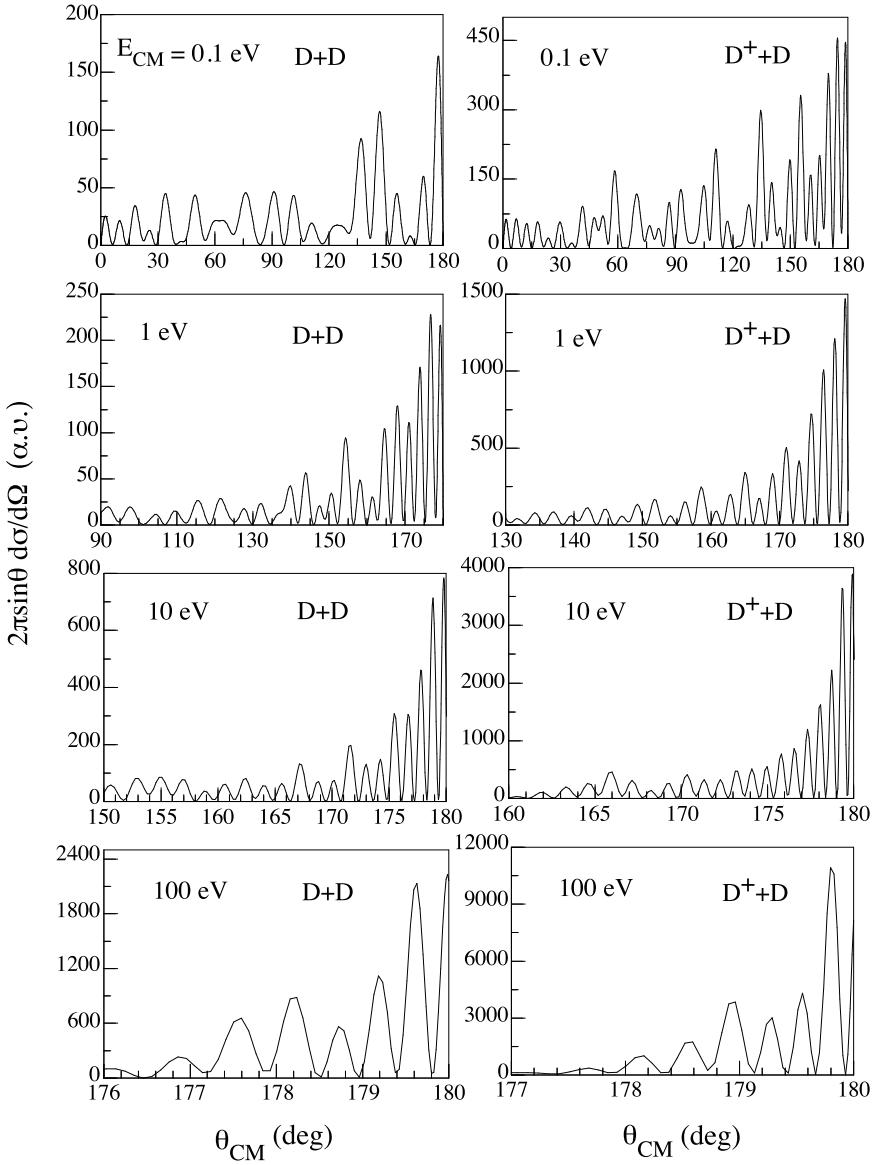


**Figure 10.** Absolute relative deviation (in %) of the integral elastic, spin-exchange, momentum transfer and viscosity cross sections in the presence of the $2p\sigma_u$–$2p\pi_u$ rotational coupling from the values in the absence of the coupling.

cross section) below it. The contribution of the large scattering angles also decreases with energy, becoming negligible around 100 eV. As a consequence, the momentum transfer cross section becomes very small at these energies.

Although we have not found any scaling relationship that can represent well the elastic differential cross section for all energies and scattering angles for the systems considered here, we have found an interesting and potentially useful scaling of four quantities that characterize the forward peak which makes the dominant contribution to the integral elastic cross section.

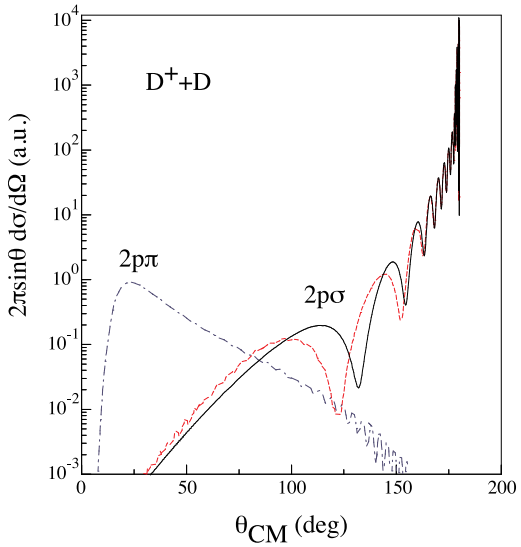


**Figure 11.** The differential cross section for spin exchange for D+D and charge transfer for $D^+ + D$, at representative CM collision energies.

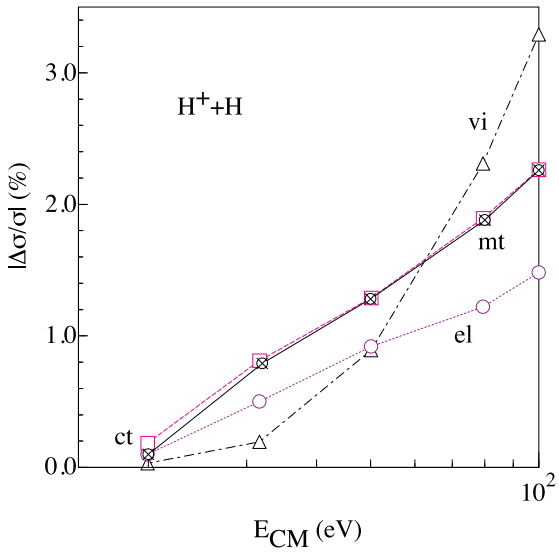


**Figure 12.** The differential cross section for charge transfer (transition into the 2p$\sigma$ state) in the absence (solid) and in the presence of the 2p$\sigma$–2p$\pi$ rotational coupling (dashed curve). The dashed-dot curve is the cross section for transition into the 2p$\pi$ state.

The first is the limiting value of the differential cross section, $\sigma_{diff}(\theta, E_{CM})$,

$$\sigma_{diff}(0, E_{CM}) = \lim_{\theta \to 0}[2\pi \sin\theta \, \mathrm{d}\sigma(\theta, E_{CM})/\mathrm{d}\Omega]. \tag{38}$$

All values of this quantity have been scaled by the reduced mass of the system to the curve that corresponds to the hydrogen projectile, i.e.

$$\sigma^A_{diff}(0, E_{CM}) = \frac{\mu_A}{\mu_0}\sigma^H_{diff}(0, E_{CM}), \tag{39}$$

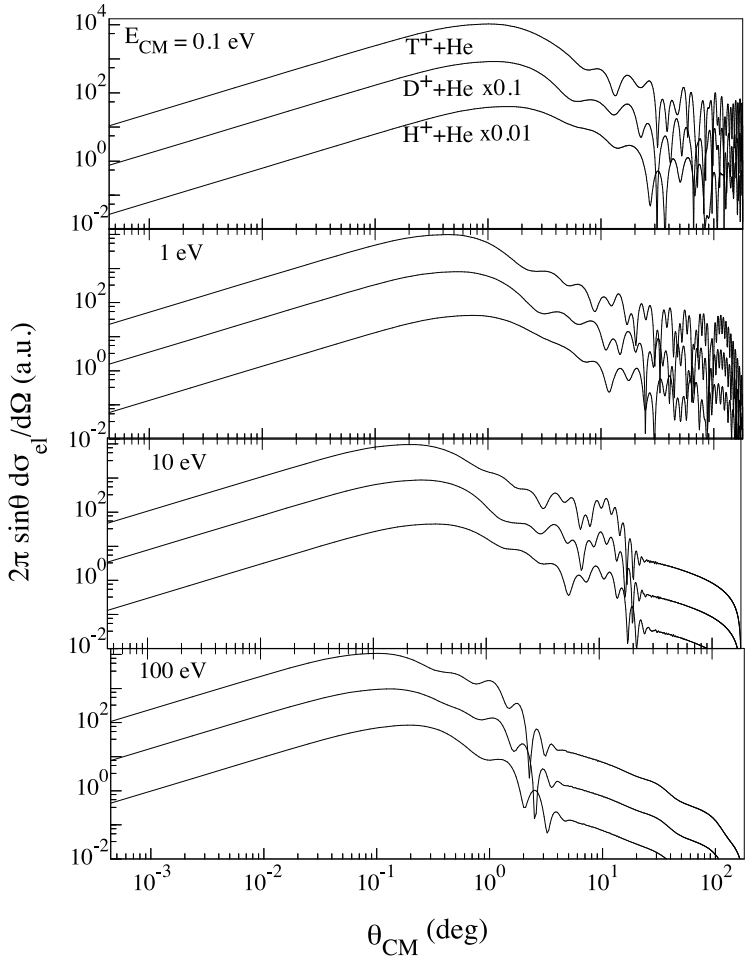


**Figure 13.** The differential elastic cross sections for $H^+$, $D^+$, $T^+$ + He collisions, at representative CM collision energies.

following the same scaling pattern with mass as the integral cross sections [2]. It is interesting, as figure 14(*a*) illustrates, that all of the scaled curves $\sigma^A_{diff}(0, E_{CM})$ for ion projectiles stay close to each other at lower energy, irrespective of the target (H, He). The next quantity is

$$\sigma_{diff}(\theta_{max}, E_{CM}) = 2\pi \sin\theta_{max}\, \mathrm{d}\sigma(\theta_{max}, E_{CM})/\mathrm{d}\Omega, \tag{40}$$

where $\theta_{max}$ is the scattering angle where the forward peak is maximum. We find that this scales as the square root of the reduced mass, i.e.

$$\sigma^A_{diff}(\theta_{max}, E_{CM}) = \sqrt{\frac{\mu_A}{\mu_0}}\sigma^H_{diff}(\theta_{max}, E_{CM}). \tag{41}$$

Values of this quantity are shown in figure 14(*b*). As can be seen in the figure, this quantity is almost constant with energy for the ion–helium systems. The value of $\theta_{max}(E_{CM})$ is presented in figure 14(*c*), and is also found to scale with reduced mass, as

$$\theta^A_{max} = \sqrt{\frac{\mu_0}{\mu_A}}\theta^H_{max} \tag{42}$$

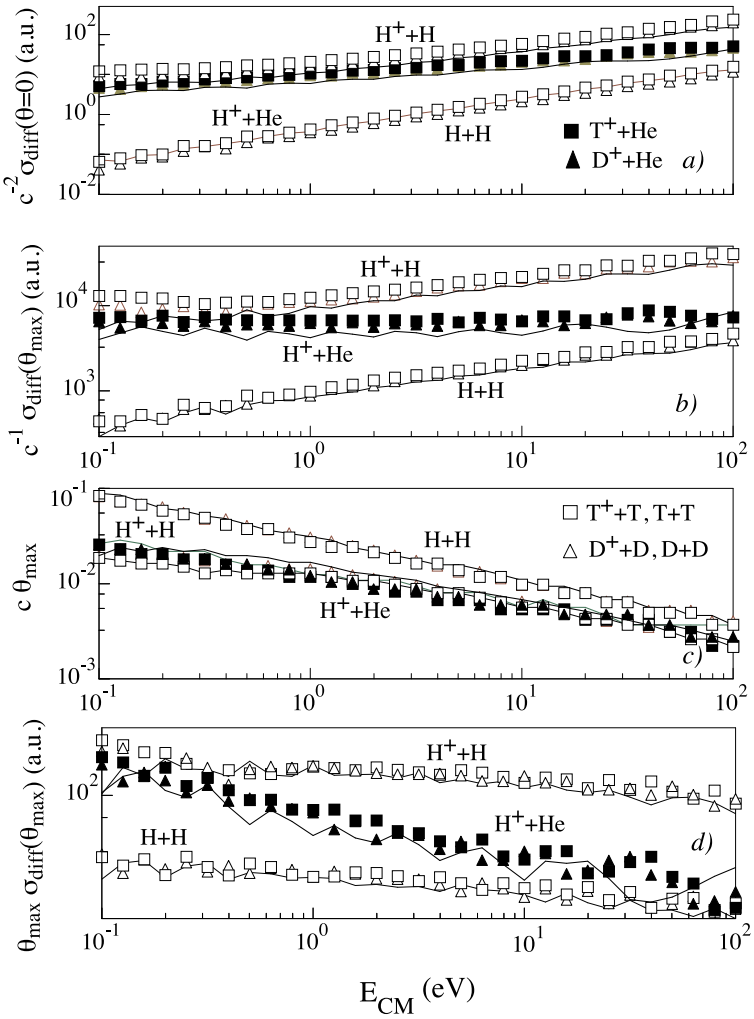


**Figure 14.** (*a*) Limiting values ($\sigma_{diff}(0, E_{CM})$) of the elastic differential cross sections at $\theta = 0$; (*b*) the peak values ($\sigma_{diff}(\theta_{max}, E_{CM})$) of the elastic differential cross sections. Scattering angle of the cross section peak (*c*) $\theta_{max}$ and (*d*) $\theta_{max}\sigma(\theta_{max}, E_{CM})$. The quantities are scaled as explained in the text.

which is inverse to the scaling of $\sigma_{diff}(\theta_{max}, E_{CM})$. As a consequence, the quantity

$$\theta^{A}_{max}\sigma^{A}_{diff}(\theta_{max}, E_{CM}) \tag{43}$$

is almost independent of mass for each of the systems considered, as seen in figure 14(*d*). Being representative of the surface area below the differential cross section, this quantity shows the same trend as a function of the collision energy as the integral elastic cross section.

## 4. Conclusions

Owing to the need for basic data for such applications as plasma physics and to fundamental interest in them, we have presented results of very accurate calculations of elastic and charge transfer (and, where applicable spin-exchange) differential and integral cross sections in slow

ion–neutral ($H^+ + H$, $D^+ + D$, $T^+ + T$, and $H^+$, $D^+$, $T^+ + He$) and neutral–neutral ($H + H$, $D + D$, and $T + T$) collisions at low (0.1–100 eV) energies. The accuracy of the results deteriorates for $E_{CM} > 20$ eV due to Coriolis coupling of the $2p\sigma_u$ and $2p\pi_u$ states as illustrated for ion–neutral systems. A similar effect to a smaller extent is expected for neutral–neutral systems. Basic features of the differential cross sections of the two types of systems have been discussed and scaling relations among quantities characterizing the forward scattering peak have been presented.

## Acknowledgments

This work has been supported by the US Department of Energy, Office of Fusion Energy Sciences, at Oak Ridge National Laboratory, managed by Lockheed Martin Energy Research Corp. under contract no DE-AC05-96OR22464.

## References

[1] Krstić P S and Schultz D R 1999 *J. Phys. B: At. Mol. Opt. Phys.* **32** 2415
[2] Krstić P S and Schultz D R 1999 *Phys. Rev.* A **60** no 3 at press
[3] Krstić P S and Schultz D R 1998 Atomic and plasma material interaction data for fusion *Nucl. Fusion Suppl.* **8**
[4] Bransden B H and McDowell M R C 1992 *Charge Exchange and the Theory of Ion–Atom Collisions* (Oxford: Clarendon)
[5] Hunter G and Kuriyan M 1980 *At. Data Nucl. Data Tables* **25** 287
[6] Helbig H F and Everhart E 1965 *Phys. Rev.* **140** A715
[7] McCarroll R and Piaccentini R D 1970 *J. Phys. B: At. Mol. Phys.* **3** 1336
[8] Landau L D and Lifshitz E M 1965 *Quantum Mechanics—Nonrelativistic Theory* (New York: Pergamon)
[9] Hirschfelder J O, Curtiss C F and Bird B B 1964 *Molecular Theory of Gases and Liquids* (New York: Wiley)
[10] Jamieson M J, Dalgarno A and Yukich J N 1992 *Phys. Rev.* A **46** 6956
[11] McDaniel E W 1964 *Collision Phenomena in Ionized Gases* (New York: Wiley)
McDaniel E W 1993 *Atomic Collisions: Heavy Particle Projectiles* (New York: Wiley)
[12] Abramowitz M and Stegun I S 1972 *Handbook of Mathematical Functions* (New York: Dover)
[13] Allison A C and Smith F J 1971 *At. Data* **3** 317
[14] Masnou-Seeuws F and Salin A 1969 *J. Phys. B: At. Mol. Phys.* **2** 1274
[15] Koyama N and Baird J C 1986 *J. Chem. Soc. Japan* **55** 801
[16] Dalgarno A 1961 *Proc. R. Soc.* **262** 132
[17] Dalgarno A and Rudge M R H 1965 *Proc. R. Soc.* A **286** 519
[18] Côté R, Dalgarno A and Jamieson M J 1994 *Phys. Rev.* A **50** 399
[19] Smith F J 1966 *Proc. Phys. Soc.* **92** 866
Smith F J 1966 *Proc. Space Sci.* **14** 929
[20] Damburg R J and Propin R Kh 1968 *J. Phys. B: At. Mol. Phys.* **1** 681
[21] Wolniewicz L 1993 *J. Chem. Phys.* **99** 1851 and references therein
[22] Schmidt M W *et al* 1993 *J. Comput. Chem.* **14** 1347
[23] Johnson B 1973 *J. Comput. Phys.* **13** 445
[24] Hunter G and Kuriyan M 1977 *Proc. R. Soc.* A **358** 321
[25] Hunter G and Kuriyan M 1977 *Proc. R. Soc.* **353** 575
[26] Hodges R R Jr and Breig E L 1991 *J. Geophys. Res.* **96** 7697
[27] Bachmann P and Reiter D 1995 *Contrib. Plasma Phys.* **35** 45
[28] Schultz D R, Ovchinnikov S Yu and Passovets S V 1995 *Atomic and Molecular Processes in Fusion Edge Plasmas* ed R K Janev (New York: Plenum) p 279
[29] Flannery M R and McCann K J 1974 *Phys. Rev.* A **9** 1947
[30] Hayden M E, Hurlimann M D and Hardy W N 1996 *Phys. Rev.* A **53** 1589